

Discrete Band-Limited Signal Reconstruction From Irregular Samples

David G. Long¹, Fellow, IEEE

Abstract—Image reconstruction from discrete samples is fundamental in remote sensing. The reconstruction problem is more complicated when the sample locations are irregularly spaced and employ different aperture functions. Further, not all 2-D sampling configurations permit full image reconstruction of band-limited signals. In this article, 2-D signal reconstruction from irregular samples with variable apertures is considered using theory and examples. Exact reconstruction requires that the signal be band-limited and the sampling matrix be invertible. The results are sensitive to the sample locations and noise in the measurements. Illustrative examples are provided using simulation and actual data from the L-band Soil Moisture Active Passive (SMAP) radiometer. The general approach can be employed with other sensors.

Index Terms—Aperture function, irregular samples, point-spread function (PSF), radiometer, reconstruction, sampling, variable aperture.

I. INTRODUCTION

A KEY challenge of satellite sensors is that they are often unable to collect measurements of the surface properties (the 2-D signal of interest) over a regular sampling grid. Instead, the measurements are irregularly spaced. A particular measurement can be expressed as the value of the convolution between the signal and the sensor's spatial measurement response function (MRF)¹ at the particular measurement location. The MRF is known but can vary from measurement to measurement due to changes in the observation geometry over the observation swath and the antenna pattern. Given the irregularly spaced measurements and varying MRF, the goal is to reconstruct the 2-D signal on a uniform grid at the finest possible resolution. Recently, a discrete reconstruction approach for the problem of irregular samples and variable aperture function was developed [1]. In this article, we generalize the method and apply it to additional sensors. We consider a wide range of parameters and address the limitations of the method, including computational issues and the effects of noise on the signal reconstruction.

Manuscript received May 9, 2020; revised June 20, 2020; accepted July 18, 2020. Date of publication September 18, 2020; date of current version April 22, 2021. This work was supported in part by NASA under Contract NNX16AN01G.

The author is with the Department of Electrical and Computer Engineering, Brigham Young University, Provo, UT 84602 USA (e-mail: long@ee.byu.edu).

Color versions of one or more of the figures in this article are available online at <https://ieeexplore.ieee.org>.

Digital Object Identifier 10.1109/TGRS.2020.3022761

¹Sometimes termed the measurement impulse response function, the point spread function (PSF), or the measurement aperture function.

This article is organized as follows: after a background section, we extend the discrete approach developed in [1] and consider the constraints on the locations of the irregular samples to ensure full reconstruction of 2-D signals. We then consider what band-limits are required for a given sampling scheme and the effects of the variable aperture function. The effects of noise are considered. An illustrative example is provided demonstrating the utility of the technique in remote sensing based on reconstruction of surface brightness temperature (T_b) images from spaceborne radiometer measurements; however, the reconstruction approach can be applied to other classes of instruments.

A. Background

A traditional approach to reconstruction from irregular samples has been to interpolate the measurements to a regular grid. The variable aperture is ignored. Once the measurements are resampled (interpolated) to a regular grid, the 2-D signal is estimated using the theory of band-limited (i.e., lowpass) signal reconstruction from uniformly spaced samples (i.e., “regular sampling”). This is a classic signal processing technique found in signal processing textbooks (e.g., [2]) that is based on the well-known Nyquist criterion that states that a signal can be reconstructed from uniform samples collected at twice the highest frequency present in the signal [3].

While relatively simple, this traditional interpolation approach introduces artifacts into the signal, has limited resolution, and ignores information about the MRF. Instead, we consider direct reconstruction from the irregular samples. In the general case of irregular sampling with an ideal delta function MRF with infinite samples, Gröchenig's lemma ensures that a band-limited signal can be exactly reconstructed from samples that are “delta dense,” that is, expressed in one dimension, the Gröchenig criteria requires that the largest space between samples be less than $\ln(2)/2\omega_0$ where ω_0 is the highest frequency [4], [5]. This is about $1/\ln(2) \approx 1.44$ times the Nyquist rate for uniform sampling [6].

In practice, only a finite number of samples are available. Without an analytic form for the signal, an arbitrary signal cannot generally be fully reconstructed from only a finite number of samples. However, the implicit assumption made when sampling a signal is that it can be accurately represented by a finite number of discrete samples. The only class of signals that can be fully represented from a finite number of samples are periodic, band-limited signals [1], [2]. Thus, even

if the underlying signal is not periodic, the act of sampling and reconstruction implicitly *requires* that the sampled signal be treated as both periodic and band-limited in order for the sampling and reconstruction to be consistent [1]. With this in mind, the problem of reconstruction of continuous band-limited signals from samples can be reduced to reconstruction of discrete periodic signals from discrete samples.

In the 1-D case, Long and Franz [1] showed that perfect band-limited reconstruction can be obtained from a minimum number of disjoint samples arbitrarily located even when the sampling aperture function varies from sample to sample. However, they also showed that for 2-D signals some sampling configurations are incapable of full signal reconstruction. In the following, their approach is generalized and explored in more detail.

II. REGULAR 1-D SAMPLING AND RECONSTRUCTION

A continuous, bounded, band-limited, periodic signal $f(t)$ with period NT (N integer) can be exactly represented by the discrete-time signal $f[n] = f(nT)$ where T is the uniform discrete sampling interval so long as the maximum frequency is less than $2/T$. Reconstruction of such signals from their samples is a classic problem in signal processing [2], [3] and trigonometric polynomial interpolation in numerical analysis [7]–[11].

The discrete Fourier transform (DFT) $F[k]$ of the periodic $f[n]$ can be written as

$$F[k] = \sum_{n=0}^{N-1} f[n] e^{-j2\pi kn/N} \quad (1)$$

where $j = \sqrt{-1}$. For $f(t)$ band-limited to frequencies less than $B = 2TM/N$, it follows that $F[k] = 0$ for all $|k| > M$. The signal $f[n]$ can be fully represented by the subset of its Fourier coefficients $\{F[k]\}$ for $|k| \leq M$

$$f[n] = \frac{1}{N} \sum_{k=0}^{2M} F[k - M] e^{j2\pi(k-M)n/N} \quad (2)$$

where M is the discrete band-limit. Then,

$$f[n] = d_a \sum_{k=0}^{2M} f_k D_{M,N}(n - kd_a) \quad (3)$$

where $d_a = N/(2M + 1)$, $f_k = f(kd_a T)$, and $D_{M,N}(\cdot)$ is the Dirichlet kernel

$$D_{M,N}(\tau) = \begin{cases} \frac{\sin(\pi \tau (2M + 1)/N)}{\sin(\pi \tau / N)}, & \tau \neq 0 \\ 2M + 1, & \text{else} \end{cases} \quad (4)$$

which is N -periodic in τ and M -band-limited [1]. The signal values $f_k = f(kd_a T)$ at discrete sample times $kd_a T$, are here termed the “maximally spaced equivalent uniform” (MSEU) samples. When d_a is an integer, then $f_k = f[kd_a]$, which is evaluated modulo N ; however, d_a is not required to be an integer.

We define the integer d ($d \leq d_a$) such that $N = d(2M + 1 + E)$ where E is also a non-negative integer, typically chosen to be the smallest possible value. E provides flexibility in

defining the relationship between N and M and d . This representation is termed the “uniform sampling interval” (USI). The integer-valued USI (d) and the MSEU (d_a), which need not be an integer, sampling intervals are related by

$$d_a = N/(2M + 1) \\ = d(2M + 1 + E)/(2M + 1) \quad (5)$$

$$d = N/(2M + 1 + E) \\ = d_a(2M + 1)/(2M + 1 + E). \quad (6)$$

When d_a is also an integer, then E can be set to zero and $d = d_a$.

The original band-limited, periodic continuous signal $f(t)$ can be computed from the MSEU of USI samples using

$$f(t) = d_a \sum_{k=0}^{2M} f(kd_a T) D_{M,N}(t/T - kd_a) \quad (7)$$

$$f(t) = d \sum_{k=0}^{2M+E} f[kd] D_{M,N}(t/T - kd). \quad (8)$$

It is noted that the MSEU representation requires $N_{\text{MSEU}} = 2M + 1$ samples while the USI representation requires $N_{\text{USI}} = N/d = 2M + 1 + E$ samples and that $N_{\text{USI}} \geq N_{\text{MSEU}}$ with equality only when $E = 0$. MSEU is thus more efficient (i.e., requires fewer sample values), but USI has the advantage of using only canonical ($t = nT$) signal values.

Our primary interest is in the discrete signal $f[n] = f(nT)$. Then,

$$f[n] = d_a \sum_{k=0}^{2M} f(kd_a T) D_{M,N}(n - kd_a) \quad (9)$$

$$f[n] = d \sum_{k=0}^{2M+E} f[kd] D_{M,N}(n - kd). \quad (10)$$

These equations can be written in matrix form as

$$\mathbf{f} = \mathbf{D}\mathbf{a} \quad (11)$$

$$\mathbf{f} = \mathbf{C}\mathbf{b} \quad (12)$$

where the N element signal vector \mathbf{f} has elements $(\mathbf{f})_n = f[n]$, the vector \mathbf{a} has $2M + 1$ elements $a_k = f(kd_a T)$, the $N \times (2M + 1)$ matrix \mathbf{D} has elements

$$(\mathbf{D})_{l,k} = d_a D_{M,N}(l - kd_a) \quad (13)$$

the discrete sampled signal \mathbf{b} has $2M + 1 + E$ elements $b_k = f[kd]$, and the $N \times (2M + 1 + E)$ matrix \mathbf{C} has elements

$$(\mathbf{C})_{l,k} = d D_{M,N}(l - kd). \quad (14)$$

Both \mathbf{D} and \mathbf{C} have rank $2M + 1$. When $E = 0$, $d_a = d$, $\mathbf{C} = \mathbf{D}$, and $\mathbf{b} = \mathbf{a}$. The vector \mathbf{b} is related to \mathbf{a} by [1]

$$\mathbf{b} = \mathbf{D}_0 \mathbf{a} \quad (15)$$

where the $(2M + 1 + E) \times (2M + 1)$ element matrix \mathbf{D}_0 is composed of a scaled subset of rows of \mathbf{D} , that is,

$$(\mathbf{D}_0)_{l,k} = d D_{M,N}(ld - kd_a). \quad (16)$$

The vector \mathbf{a} is related to \mathbf{b} by the $(2M + 1) \times (2M + 1 + E)$ element matrix \mathbf{D}_1

$$\mathbf{a} = \mathbf{D}_1 \mathbf{b} \quad (17)$$

where $\mathbf{D}_1 = (d_a/d)\mathbf{D}_0^T$ has elements

$$(\mathbf{D}_1)_{k,l} = d_a D_{M,N}(ld - kd_a). \quad (18)$$

Note that \mathbf{D}_1 is the Moore-Penrose pseudo inverse of \mathbf{D}_0 !

A. Irregular 1-D Sampling and Reconstruction

Suppose that $N_s \geq 2M + 1$ samples of one period of $f[n]$ are available at an arbitrary but unique set of locations $n_m \in \{n_1, \dots, n_{N_s}\}$. The samples can be at irregular sample spacings. Long and Franz [1] showed that $f[n]$ can be perfectly reconstructed from these samples. Here we extend the analysis.

Let \mathbf{f}_s be the N_s element vector of the samples, that is,

$$(\mathbf{f}_s)_m = f[n_m]. \quad (19)$$

It is noted that \mathbf{f}_s can be written in terms of \mathbf{b} or \mathbf{a} using

$$\mathbf{f}_s = \mathbf{C}_\Delta \mathbf{b} \quad (20)$$

$$\mathbf{f}_s = \mathbf{D}_\Delta \mathbf{a} \quad (21)$$

where \mathbf{C}_Δ and \mathbf{D}_Δ are composed of a subset of rows of \mathbf{C} or \mathbf{D} , respectively, that is,

$$(\mathbf{C}_\Delta)_{m,k} = d D_{M,N}(n_m d - kd) \quad (22)$$

$$(\mathbf{D}_\Delta)_{m,k} = d_a D_{M,N}(n_m d - kd_a). \quad (23)$$

Then, \mathbf{a} and \mathbf{b} can be computed by solving the linear system in (20) and (21), respectively. Once \mathbf{b} or \mathbf{a} is computed, \mathbf{f} can be computed using (11) or (12). In combined form

$$\mathbf{f}_s = \mathbf{C}_\delta \mathbf{f} \quad (24)$$

$$\mathbf{f}_s = \mathbf{D}_\delta \mathbf{f} \quad (25)$$

where $\mathbf{C}_\delta = \mathbf{C}_\Delta \mathbf{C}^{-1}$ and $\mathbf{D}_\delta = \mathbf{D}_\Delta \mathbf{D}^{-1}$. It is noted that $\mathbf{C}^{-1} = \mathbf{C}^T$ and $\mathbf{D}^{-1} = \mathbf{D}^T$.

If the sample locations n_m correspond to $n_m = md$, that is, regular sampling, then $\mathbf{f}_s = \mathbf{a} = \mathbf{b}$. In this case, the signal can be directly reconstructed using (11) with $\mathbf{C} = \mathbf{C}_\Delta$.

The solution to the linear systems in (20) and (21) can be written as

$$\mathbf{a} = \mathbf{D}_\Delta^\dagger \mathbf{f}_s \quad (26)$$

$$\mathbf{b} = \mathbf{C}_\Delta^\dagger \mathbf{f}_s = \mathbf{D}_0 \mathbf{D}_\Delta^\dagger \mathbf{f}_s \quad (27)$$

where \dagger denotes the Moore-Penrose pseudo inverse. In irregular sampling configurations the pseudoinverse of \mathbf{C}_Δ must be computed numerically.

In the 1-D case, a band-limited, periodic $f[n]$ can be perfectly reconstructed from a set of $N_s \geq 2M + 1$ irregular samples $f[n_i]$ for arbitrary n_k , so long as the samples are distinct $n_k \bmod N$ [1], [5]. This means that the samples can be anywhere within the signal period without any requirements for spacing. In minimum samples case, when $N_s = 2M + 1$, \mathbf{D}_Δ is square and invertable, that is, $\mathbf{D}_\Delta^\dagger = \mathbf{D}_\Delta^{-1}$ and $\mathbf{C}_\Delta^\dagger = \mathbf{D}_0 \mathbf{D}_\Delta^{-1}$. When ‘‘extra’’ samples are available, that is, $N_s > 2M + 1$, they contribute to noise reduction in the reconstructed signal [1].

B. Variable Apertures

In practice, measurements are collected as the weighted average of the signal over an interval. The weighting function is known as the aperture function or PSF. In one dimension for an aperture function $v_i[n]$, the i th observation centered at n_i is modeled as the value $g_i[n_i]$ of $g_i[n] = v_i[n] * f[n]$ where $*$ denotes discrete convolution. When the aperture function is fixed, that is, $v_i[n]$ is the same for all i , the observations $g_i[n_i]$ can be used to first reconstruct a signal $g[n]$, then $f[n]$ is computed using signal deconvolution techniques to compute $f[n]$ from $g[n]$. The signal $f[n]$ can be exactly computed from $g[n]$ so long as the aperture spectrum does not have any nulls over the bandwidth of the signal spectrum [1].

When the aperture is variable, that is, is different for different measurements—sometimes termed a shift-variant PSF, this deconvolution approach to reconstruction cannot be used. Instead, the variable aperture sampling matrix is created and inverted to estimate the equivalent uniform samples of f_k directly from the $g_i[n_i]$ [1].

Assuming $v_i[n]$ is reasonably well-behaved, the observations (measurements) are

$$g_i[n_i] = (v_i[n] * f[n])|_{n_i} = \sum_{m=0}^{N-1} f[m] v_i[n_i - m] \\ = \sum_{m=0}^{N-1} \sum_{k=0}^{2M+E} f_k D_{M,N}(m - kd) v_i[n_i - m] \quad (28)$$

where again, $f_k = f(kdT) = f[kd]$. In matrix form with USI, the aperture-filtered measurements can be expressed as

$$\mathbf{g} = \mathbf{C}_V \mathbf{b} = \mathbf{C}_V \mathbf{C}^{-1} \mathbf{f} = \mathbf{C}_v \mathbf{f} \quad (29)$$

where $(\mathbf{g})_i = g_i[n_i]$, \mathbf{C}_V is the $N_s \times (2M + 1 + E)$ sampling matrix whose i th row is the convolution of the Dirichlet kernel and the aperture function $v_i[n]$ sampled at n_i , and $\mathbf{C}_v = \mathbf{C}_V \mathbf{C}^{-1} = \mathbf{C}_v \mathbf{C}^T$. The vector \mathbf{b} or the signal \mathbf{f} is computed by inverting (29), assuming the variable aperture sampling matrix \mathbf{C}_V is invertable [1]. When \mathbf{C}_V is not invertable, an approximate result can be obtained using the pseudo inverse.

III. 2-D SAMPLING AND RECONSTRUCTION

With an important and subtle distinction, the ideas in Section II can be extended to two dimensions where a 2-D signal $f(t_r, t_c)$ that is periodic with a 2-D period $[N_1 T_1, N_2 T_2]$ (N_1 and N_2 integers) and uniform sample spacings T_1 and T_2 can be represented by the discrete pixel image $f[r, c] = f(rT_1, cT_2)$. The 2-D DFT $F[k_1, k_2]$ of $f[r, c]$ is

$$F[k_1, k_2] = \sum_{r=0}^{N_1-1} \sum_{c=0}^{N_2-1} f[r, c] e^{-j2\pi k_1 r/N_1} e^{-j2\pi k_2 c/N_2}. \quad (30)$$

The 2-D band-limit is a rectangular region of support in the frequency domain where $F[k_1, k_2] = 0$ for $|k_1| > M_1$ or $|k_2| > M_2$. It is noted that there are only N_r , where $N_r = R_1 R_2$ with $R_1 = 2M_1 + 1$ and $R_2 = 2M_2 + 1$, non-zero entries in $F[k_1, k_2]$. Thus, it is a necessary, but not sufficient,

condition that at least N_r samples of f are required to fully reconstruct the $[M_1, M_2]$ -band-limited f .

We are interest primarily in the USI representation. Following the USI 1-D case, an arbitrary $[M_1, M_2]$ -band-limited discrete 2-D signal $f[n_1, n_2]$ can be written in terms of its USI samples as

$$f[n_1, n_2] = \sum_{p_1=0}^{2M_1+E_1} \sum_{p_2=0}^{2M_2+E_2} f[n_1 d_1, n_2 d_2] \times D_{M_1, N_1}(n_1 - p_1 d_1) D_{M_2, N_2}(n_2 - p_2 d_2) \quad (31)$$

where $d_1 = N_1/(R_1 + E_1)$ and $d_2 = N_2/(R_2 + E_2)$ are positive integers and where E_1 and E_2 are nonnegative integers. For later use, $d_{a1} = N_1/R_1 = N_1/(2M_1 + 1)$, $d_{a2} = N_2/R_2 = N_2/(2M_2 + 1)$, $N_m = (R_1 + E_1)(R_2 + E_2)$, and $N_N = N_1 N_2$.

In matrix-vector notation,² the 2-D equivalent to (11) and (12) are

$$\mathbf{f} = \mathbf{C}\mathbf{b} \quad (32)$$

$$\mathbf{f} = \mathbf{D}\mathbf{a} \quad (33)$$

where \mathbf{b} is a N_m element vector with $(\mathbf{b})_p = f[p_1 d_1, p_2 d_2]$, $p = p_2(R_1 + E_1) + p_1$, \mathbf{a} is a N_r element vector, \mathbf{C} is an $N_N \times N_m$ element matrix, and \mathbf{D} is an $N_N \times N_r$ element matrix of sampled Dirichlet kernels where

$$(\mathbf{C})_{k,l} = D_{M_1, N_1}(n_1 - p_1 d_1) D_{M_2, N_2}(n_2 - p_2 d_2) \quad (34)$$

$$(\mathbf{D})_{k,m} = D_{M_1, N_1}(n_2 - q_1 d_{a1}) D_{M_2, N_2}(n_2 - q_2 d_{a2}) \quad (35)$$

with $k = n_2 N_1 + n_1$, $l = p_2(R_1 + E_1) + p_1$, and $m = q_2 R_1 + q_1$. While the values \mathbf{b} correspond to canonical locations, that is, $(\mathbf{b})_m = f[q_1, q_2]$, when either E_1 or E_2 are non-zero, vector \mathbf{a} does not correspond to values on the canonical grid.

The vectors \mathbf{a} and \mathbf{b} are related by [see (15)]

$$\mathbf{b} = \mathbf{D}_o \mathbf{a} \quad (36)$$

where \mathbf{D}_o is composed of a subset of rows of \mathbf{D} , that is,

$$(\mathbf{D}_o)_{k,l} = d_{a1} D_{M_1, N_1}(n_1 d - p_1 d_a) d_{a2} D_{M_2, N_2}(n_2 d - p_2 d_a). \quad (37)$$

In matrix form, the 2-D equivalent of the variable aperture sampling matrix in 29 can be written in similar form

$$\mathbf{g} = \mathbf{C}_V \mathbf{b} = \mathbf{C}_v \mathbf{f} \quad (38)$$

where \mathbf{g} is the vector of measurements, \mathbf{b} is the vectorized subsampled image, \mathbf{f} is the full vectorized image, \mathbf{C}_V is the subsampled variable aperture sampling matrix, and \mathbf{C}_v is the full variable aperture sampling matrix where the rows of \mathbf{C}_V and \mathbf{C}_v contain the vectorized result of convolving the 2-D aperture functions $v_k[r, c]$ with the 2-D Dirichlet function [1].

To fully reconstruct the signal from the samples, a minimum of N_r unique³ samples are required. Suppose $N_s \geq N_r$ unique samples of $f[n_1, n_2]$ are available. Are the N_s samples capable of supporting full reconstruction of the original signal?

²For row-major vectorization the i th element of the vector \mathbf{f} is $\mathbf{f}_i = f[r, c]$ where $i = r + cN_1$ for an $N_1 \times N_2$ image f [1].

³Canonical sample locations $f(n_1 T, n_2 T) = f[n_1, n_2]$ that are disjoint modulo the 2-D period.

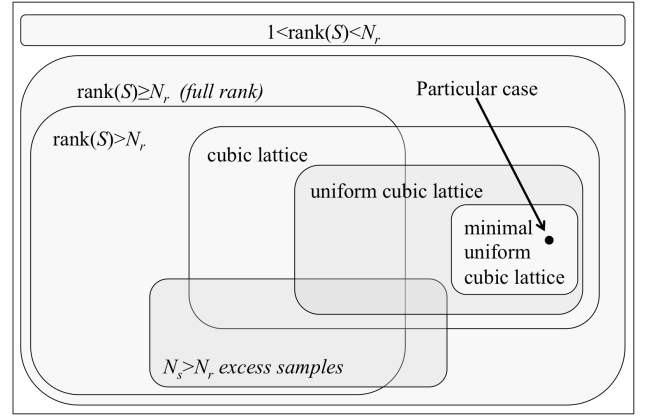


Fig. 1. Illustration of the relationship of the various 2-D signal sampling spaces. S is the sampling matrix where $S = \mathbf{C}_\Delta$, $S = \mathbf{D}_\Delta$, or $S = \mathbf{C}_V$ according to the problem, and $\text{rank}(S)$ refers to the column rank of S .

If the samples locations are a cubic lattice sampling (either regular or irregular), the answer is yes. But for more general irregular samples this may not be the case, for either ideal or variable aperture functions [1].

If the sampling matrix (\mathbf{D} , \mathbf{C} , or \mathbf{C}_V depending on the particular case) is not invertable, then the image cannot be precisely reconstructed from the samples, though pseudo inverses can be used. Section IV focuses on this case.

IV. LIMITS OF 2-D RECONSTRUCTIONS

Unlike 1-D reconstruction, 2-D reconstruction is not always possible for arbitrarily located samples [1]. Accurate 2-D reconstruction imposes restrictions on the sample locations to insure that the sample matrix \mathbf{D} is full band-limited (column) rank [9].

In conventional sampling theory, the samples are uniformly spaced in two dimensions. This is an example of the more general “generalized cubic lattice⁴” sampling scheme that is defined as the cross product of two 1-D samplings, one along each dimension [12].

Sample locations on a generalized cubic lattice location scheme are always full band-limited rank [10], [11], even if the lattice spacing is nonuniform [1]. Though no simple statement of the requirements for irregular 2-D sampling for band-limited reconstruction is available, the reconstructability of a particular set of sample locations can be tested by evaluating the rank of the sampling matrix [1], [9]. If \mathbf{D} has full column rank or \mathbf{C} has column rank $N_r = R_1 R_2$ (which at a minimum requires $N_s \geq N_r$), \mathbf{a} and \mathbf{b} can be uniquely computed from \mathbf{f}_s .

While \mathbf{C} is always full column rank for generalized cubic lattice sampling, for more general sampling distributions, it is not guaranteed to be full column rank [1]. It is noted that the rank of \mathbf{C} is dependent only on the sample locations and not on the sample values.

⁴For R_1 distinct sample indexes $(n_1)_i \in \{0, \dots, N_1 - 1\}$ and R_2 distinct sample indexes $(n_2)_j \in \{0, \dots, N_2 - 1\}$, a cubic lattice consists of $N_r = R_1 R_2$ samples located at $n_{i,j} = [(n_1)_i, (n_2)_j]$. A regular or “uniform cubic lattice” has $(n_1)_i = i d_1$ and $(n_2)_j = j d_2$.

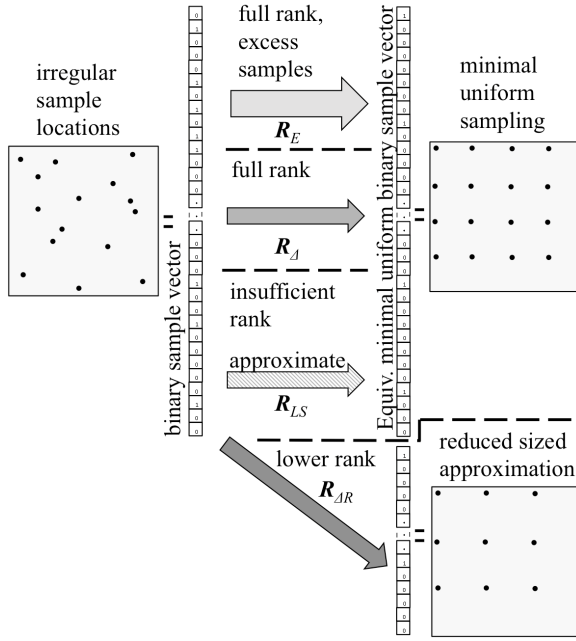


Fig. 2. Illustration of the relationship of the various 2-D signal sampling spaces. Discrete sample locations are represented by dots, which have a corresponding binary representation. In effect, irregular sample reconstruction converts the irregular binary sampling location vector to a regular binary sampling location vector.

To better understand the conditions for reconstructability, Fig. 1 illustrates the relationship of various sampling spaces in 2-D sampling and reconstruction of a band-limited signal. It is noted that if the column range of the sampling matrix ($S = \mathcal{C}_\Delta$, $S = \mathcal{D}_\Delta$, or $S = \mathcal{C}_V$ as appropriate for the case of interest) is less than the minimum number of samples N_r , the signal cannot be reconstructed. Only if the rank of S is greater than or equal to N_r , is it possible to fully reconstruct the signal. When this is true, the N_s samples can be uniquely mapped to a particular uniform cubic lattice sampling. There is a set of possible minimum uniform cubic lattice samplings. For this article, we arbitrarily choose the particular uniform cubic lattice sampling origin at $(n_1, n_2) = (0, 0)$. However, any origin n_1, n_2 with $n_1 \in [0 \dots d_1 - 1]$ and $n_2 \in [0 \dots d_2 - 1]$ can be used. Signal representation at all other samplings can be derived from this USI set. Recall that a cubic lattice sampling of adequate dimension is always full rank, even if irregular [1].

Fig. 2 illustrates the processing flow in the reconstruction from irregular samples to USI representation from which the full signal can be reconstructed. The 2-D sampling locations are shown as dots in one period of the signal. These locations can be represented as binary vector with 1 for a sample at the corresponding location and 0 for no sample. The irregular sample locations are mapped to a uniform cubic lattice sampling via the reconstruction process, indicated by $\mathbf{R} = S^\dagger$ matrices. When the sampling matrix is full band-limited rank ($\text{rank}(S) > N_r$, \mathbf{R}_E), or ($\text{rank}(S) = N_r$, \mathbf{R}_Δ), full USI or MSEU representations can be computed. When the sampling matrix is not full band-limited rank ($\text{rank}(S) < N_r$), only a reduced-rank approximation of the signal can be computed. This can be represented by a smoothed (\mathbf{R}_{LS}) solution or a

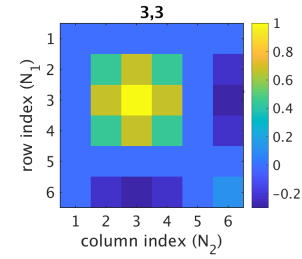


Fig. 3. Spatial response function corresponding to an ideal sample at a particular location (3, 3) within a 2-D $M_1 = M_2 = 1$ band-limited $N_1 = N_2 = 6$ periodic signal. The label at top indicates the row, column address of the sample location.

reduced order, that is, smaller M_1 and/or M_2 , USI representation ($\mathbf{R}_{\Delta R}$) which could be over sampled at the reduced order. The latter requires reselection of the reconstruction parameters and recomputation of the corresponding \mathcal{D} , \mathcal{C} , or \mathcal{C}_V matrices.

A. Illustrative Toy Problem

To help appreciate the issues associated with 2-D reconstruction, a simple toy problem with $M_1 = M_2 = 1$, $d_1 = d_2 = 1$, and $E_1 = E_2 = 0$ with an ideal (delta function)⁵ aperture function is considered. For this case, the USI and MSEU representation are identical with $N_1 = N_2 = 6$ so that $\mathcal{C} = \mathcal{D}$ for this case. The minimum number of samples required for full reconstruction is $N_s = N_r = 9$.

For these parameters there are 94 143 280 permutations of the sample locations (36 possible unique sample locations taken 9 at a time). Of these possible samplings, 400 are cubic lattice samples. Of all the sample location permutations, 54 781 216 (58.19%) produce full band-limited rank sample matrices based on exhaustive numerical computation.

The spatial response function corresponding to a particular sample is a 2-D Dirichlet function, illustrated for a particular sample location at 3,3 in Fig. 3. Fig. 4 shows four particular sampling schemes: Fig. 4(a) shows ideal, regular sampling, Fig. 4(b) shows a closely space cubic sampling, and Fig. 4(c) shows an irregular sampling. All of these produce full band-limited rank sample matrices so that the band-limited signal can be exactly reconstructed from the samples. However, moving only a single sample in Fig. 4(c) to produce Fig. 4(d) results in a sample matrices which is not full rank and therefore is unable to fully reconstruct the signal.

Fig. 5 shows the full sampling matrices (\mathcal{D}) associated with the sampling schemes in Fig. 4. The corresponding spatial response functions (which correspond to the columns of the plot of S in Fig. 5) are shown in Fig. 6. It is noted that these are identical Dirichlet functions shifted to be centered at each sample location. Fig. 7 illustrates the reduced sampling matrices (\mathcal{D}_Δ matrices) associated with the sampling schemes in Fig. 4. For the ideal uniform sampling, \mathcal{D}_Δ is an identity matrix. It is noted that the condition number of the irregular sampling case Fig. 5(c) is better than the closely spaced cubic lattice sampling in Fig. 5(b).

⁵Note that a discrete delta function is equivalent to a Dirichlet function in the band-limited space.

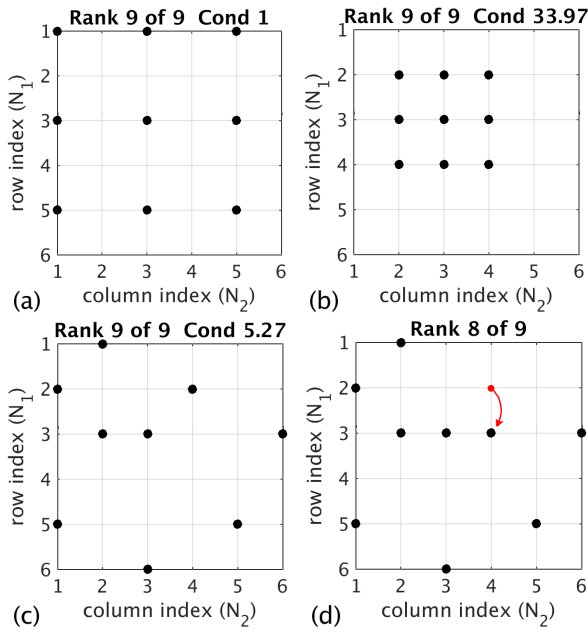


Fig. 4. Maps of the locations of four sets of samples for an $N_1 = N_2 = 6$ periodic signal. (a) Ideal regular sampling. (b) Particular cubic lattice sampling. (c) Particular full-rank irregular sampling. (d) Non-full-rank irregular sampling resulting from moving one sample location in (c).

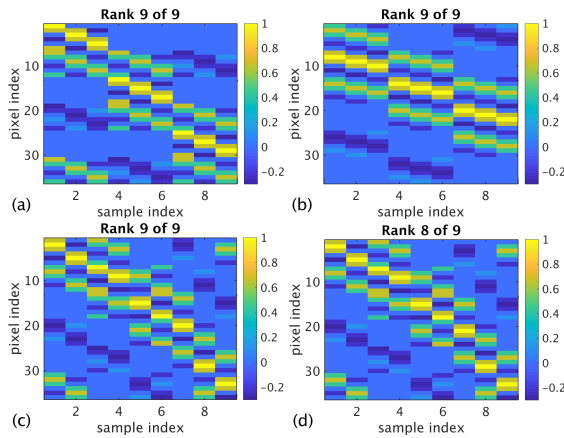


Fig. 5. Full sampling matrices for each of the sampling cases in Fig. 4. For convenience, the image shows the transpose of the sampling matrix.

To illustrate the effects of a varying aperture in this toy problem, one of two different apertures are randomly assigned to each sample location, and the reduced variable aperture sampling matrix is computed. Fig. 8(a) illustrates the two apertures and which of the samples are assigned to which aperture. One aperture is wider while the other is narrower, but both span multiple pixels. The corresponding sample matrix and the components of the full sample matrix are shown in Fig. 8(b) and (c), respectively. In practice the aperture functions do not change the matrix rank, so the original signal can be fully recovered, but they can modify the matrix condition number either smaller or larger. In this particular case, the aperture functions increase the matrix condition number, which can degrade the numerical accuracy of the

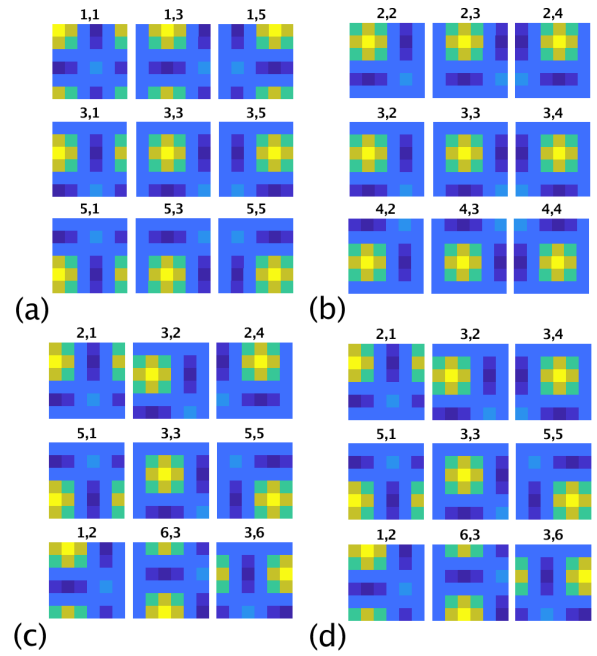


Fig. 6. Individual sample response functions for each sample for each of the sampling cases in Fig. 4. Compare with Fig. 3. The label at top indicates the row, column address of the sample location.

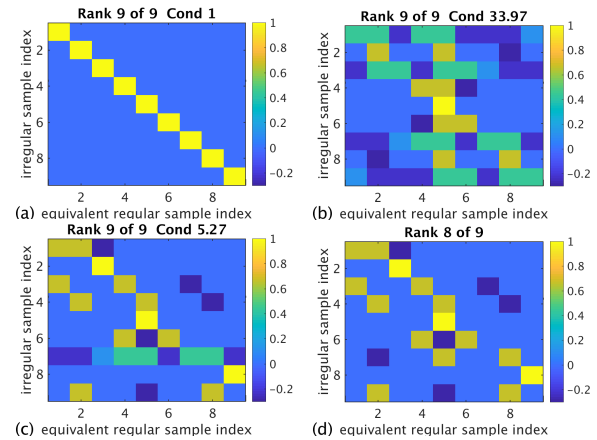


Fig. 7. Reduced sampling matrices (\mathcal{D}_Δ) for each of the sampling cases in Fig. 4. It is noted that in the non-full rank case, four rows of \mathcal{D}_Δ matrix (which correspond to 4 different sample locations) are interdependent. For this case, for example the fourth row can be written as 1.5 times the fifth row minus the seventh row pulse one-half of the last row.

reconstruction. Since a large condition number implies the inverse is sensitive to numerical computation errors, poor condition numbers can limit the practical implementation of the approach even though the matrix is known to be invertable. We note that both the rank and condition numbers are functions only of the sample locations and aperture functions, and not of the signal values.

To gain insight into how frequently non-full rank sampling matrices are encountered when $N_s = N_r$, a simple Monte Carlo experiment is performed. Square images are employed with $M_1 = M_2$, $N_1 = N_2$, and $d_1 = d_2$. Two aperture functions were considered: an ideal aperture (a δ function)

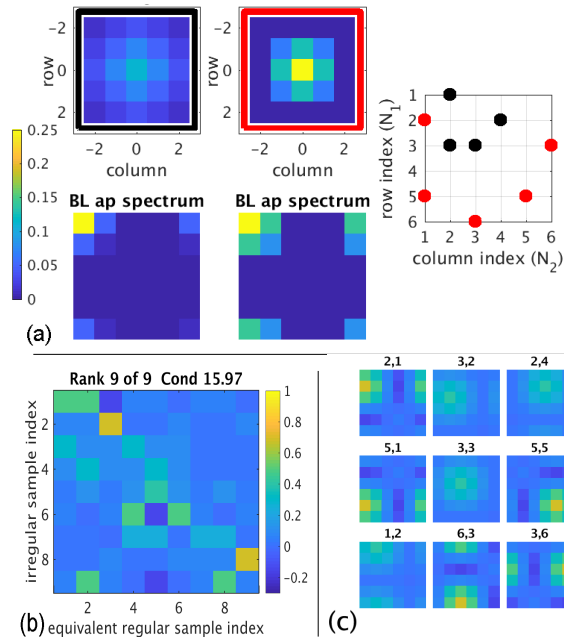


Fig. 8. Variable aperture result. (a) [Top left] Images of two different apertures consisting of Fejer (triangle) windows of different sizes. (Bottom left) Fourier transform of the bandpass filtered aperture functions. (Top right) Locations of sample centers. Colors of each spot correspond to the aperture function used at that location. (b) \mathcal{D}_Δ matrix for this case. Compare to Fig. 7(c). (c) Individual sample response functions for each sample. Compare to Fig. 6(c).

and a Fejer (triangle function) aperture. For a given value of M_1 multiple $N_1 > 2M_1 + 1$ values are considered, with d_1 computed as $d_1 = N_1 / (2M_1 + 1)$. For each case, 5000 different random sampling patterns are chosen. Each sampling realization consists of $N_s = (2M_1 + 1)^2$ unique locations selected with a uniform distribution over the $N_1 \times N_2$ image area. The reduced sampling matrix is separately evaluated for both aperture cases, and the rank for each is computed. When the matrix is full rank, the matrix condition number is also computed. The number of full-rank matrices for each case is determined, as well as the average matrix condition number of the full rank sampling matrices. The results of the experiment are shown in Fig. 9. For reference, Fig. 9(a) plots N_1 versus d_1 for various M_1 values.

As shown in Fig. 9(b), for a given value of M_1 , the percentage of full-rank \mathcal{D}_Δ matrices increases with d_1 . For large d_1 and/or large M_1 , the matrix is almost always full rank for both aperture cases. Unfortunately, as shown in Fig. 9(c) increasing M_1 or d_1 tends to increase the condition number of the sampling matrix, at least until it plateaus. The non-ideal aperture improves the condition number for small d_1 , but has little effect for larger d_1 . As M_1 is increased, the condition number becomes very large, suggesting that numerical issues can be expected to be important for larger problems. Ameliorating this is discussed in Section VIII.

V. SELECTION OF RECONSTRUCTION PARAMETERS

Ideally, the reconstruction parameters (period, sample spacing, and band-limit) of the periodic signal are known from

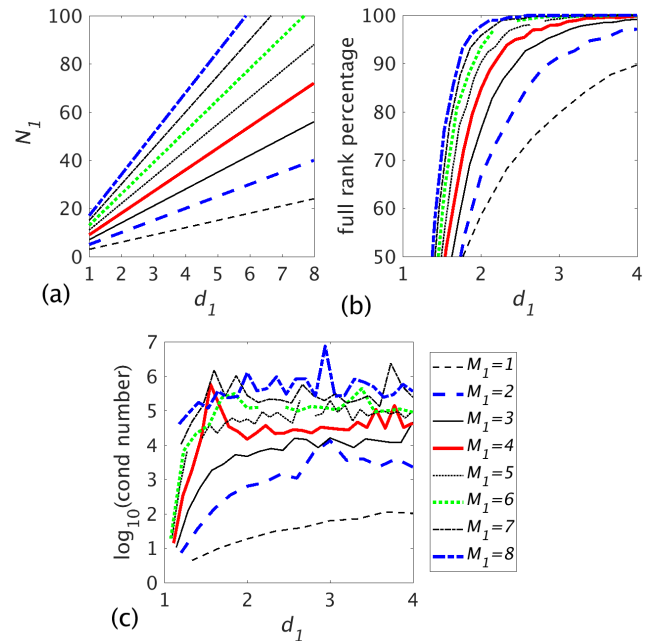


Fig. 9. Effects of d_1 on the image size, reconstruction matrix rank, and reconstruction matrix condition number. (a) Plot of N_1 versus d_1 for different values of M_1 . (b) Estimated percentage of random samplings that are full rank versus d_1 for different values of M_1 . (c) Average sampling matrix condition number versus d_1 for different values of M_1 . For computing averages, 5000 different uniformly distributed random sampling configurations were generated for each case.

the problem. When not known, the user must subjectively select appropriate parameters, and there is no single answer. The following parameter selection discussion focuses on 2-D signals. With N_s samples, the $N_s \times N_N$ sample matrix \mathcal{D} is considered full band-limited rank if the rank of \mathcal{D} , denoted by r , is greater than or equal to N_r . This indicates that \mathcal{D} can be inverted within the $(2M_1 + 1) \times (2M_2 + 1)$ region of frequency support for the signal.

A. Band-Limit

A fundamental assumption in reconstruction of a signal or image from its samples is that signal can be accurately represented by the samples. If this assumption is invalid, then only an approximation of the original signal can be generated from the samples. In this latter case, a variety of least-squares and other metric-based techniques must be used. It is noted that even if the underlying signal is not periodic, it can be treated as periodic by extension with proper treatment of the boundaries [1].

Two key questions then arise: In the general case: 1) what are the minimum requirements for the discrete sampling to reconstruct the signal for a given band-limit? 2) what assumptions must be made about the signal band-limit to enable full reconstruction for a given sampling configuration?

The short answer to 1) is that the sampling matrix must be invertible, that is, for an N_1, N_2 -periodic signal with a M_1, M_2 -order band-limit, the sampling matrix \mathcal{D} must have rank $r \geq N_r$. We can choose M_1 and M_2 to ensure that \mathcal{D} is full rank.

Answering question 2) can be more difficult. If only the sample locations of the finite number of samples are known, then the reconstruction parameters (N_1 , N_2 , M_1 , and M_2) must be inferred from the sample locations. Unfortunately, this is a poorly-posed problem since there can be multiple solutions.

B. Known Period

Problem 2) is considerably simplified if the period (N_1 and N_2) is known. Then, the upper limits of M_1 and M_2 can be inferred from the sample locations. A particular methodology for determining the maximum M_1 and M_2 is based on an iterative search that begins with an initial estimate for M_1 and M_2 that is used to compute the rank of the resulting sampling matrix. If the resulting sampling rank is full-rank, the values of M_1 and M_2 can be increased and the sampling matrix rank tested again. Otherwise, the values are decreased. This is repeated to find the largest M_1 and M_2 for which the sampling matrix is full rank. The resulting values are then the maximum band-limit for a reconstructable signal for the particular sampling. $E_1 \geq 0$ and $E_2 \geq 0$ are selected such that $d_1 \geq 1$ and $d_2 \geq 1$, where all the parameters are integers. This can require a computationally taxing search algorithm for large values of the parameters.

C. Unknown Period

What if the signal period is not known? Without prior knowledge of the reconstruction parameters (i.e., M_1 , M_2 , N_1 , N_2 , E_1 , and E_2), the reconstructions values must be subjectively chosen subject to the constraint that the d_1 and d_2 parameters are all integers.

An initial guess for the period can be selected from the span of the samples, that is, N_1 is set to the range of the column indices and N_2 is set to the range of row indices of the samples. Empirical results suggest that expanding the period slightly can improve overall results, as well as offer more potential solutions. Having selected the period, the algorithm for finding M_1 and M_2 previously described is then followed. If a square region of support is assumed, that is, $M_1 = M_2$, then the maximum value of M_1 for which the signal can be reconstructed is $M_1 = \lfloor (\sqrt{r} - 1)/2 \rfloor$, where $\lfloor \cdot \rfloor$ is the integer-valued ‘‘floor function,’’ that is, the largest integer less than or equal to its argument. If an appropriate M cannot be found, N_1 and N_2 must be modified and the process repeated until satisfactory parameters are found.

VI. MEASUREMENT NOISE CONSIDERATIONS

Since measurements contain noise, the effects of the noise must be considered. The samples can be modeled as noise-free signal samples plus noise, which is herein treated as independent of the signal. The noisy signal reconstruction is

$$\mathbf{g}'_s = \mathbf{g}_s + \eta_s \quad (39)$$

where \mathbf{g}'_s is the vector of noisy observations of the signal samples \mathbf{g}_s and η_s is the vector of noise added to the signal samples. The noisy reconstruction $\hat{\mathbf{f}}$ consists of the reconstructed signal plus a noise component

$$\hat{\mathbf{f}} = \mathbf{C}_v^\dagger \mathbf{g}_s + \mathbf{C}_v^\dagger \eta_s = \mathbf{C}_v^\dagger \mathbf{g}_s + \eta_D \quad (40)$$

where $\eta_D = \mathbf{C}_v^{-\text{dagger}} \eta_s$ is the net effective noise added to the reconstructed signal. It is noted that $\eta_D = \mathbf{C}_v^\dagger \mathbf{C} \mathbf{b}_\eta$ where \mathbf{b}_η is the noise spectral representation. It is thus apparent that the original noise properties are modified by the reconstruction which can amplify some components of the noise depending on the precise sampling locations and their corresponding aperture functions. Typically noise components outside of the signal band-limit defined by \mathbf{C} are eliminated. As can be expected, oversampling tends to reduce noise amplification since the additional noise samples tend to average the noise effects.

VII. APPLICATION EXAMPLE

To illustrate how reconstruction can be applied to a real sensor, radiometer brightness temperature (T_b) measurements [13] from the Soil Moisture Active Passive (SMAP) radiometer are considered. The L-band (1.41 GHz), 24-MHz bandwidth SMAP radiometer collects T_b measurements at multiple polarizations with a total radiometric uncertainty of 1.3 K [14]. The nominal 3-dB footprint size on the surface is 39 km \times 47 km, an area of approximately 1833 km². The spacecraft movement, rotating antenna and measurement timing results in an irregular sampling of the surface with overlapping measurements spaced approximately 11 km apart in the rotation direction, with nominally 31 km between rotations [15].

A SMAP T_b measurement is the average over the measurement period of the integral of the product of the surface brightness response $T_b(x, y)$ and the antenna pattern, which can be expressed as

$$z_n = \frac{1}{\overline{G}_n} \iint T_b(x, y) G_n(x, y) dx dy \quad (41)$$

with

$$\overline{G}_n = \iint G_n(x, y) dx dy, \quad (42)$$

where $G_n(x, y)$ is the time-averaged antenna pattern for the i th measurement, that is, the MRF. The SMAP MRF can be modeled with an elliptical Gaussian function whose 3-dB (half-power) point matches the footprint size [15]. The orientation of the ellipse varies over the swath according to the azimuth antenna angle when the measurement was collected, and so varies with measurement location. The Gaussian response is clipped when it falls below -30 dB of the peak.

Given a set of measurements z_n we desire to estimate the surface brightness temperature T_b over a discrete, uniformly spaced, fine resolution grid with spacing $T = 8.9$ km. The measurement center locations (at $x = n_1 d_1 T$, $y = n_2 d_2 T$) and corresponding MRF are discretized to this grid for $i \in [1 \dots N_1]$ and $l \in [1 \dots N_2]$. Following the earlier discussion, T_b is treated as band-limited and periodic over the region. The measurement model is

$$z_n = \sum_i \sum_l (G_n)_{i,j} T_b(i d_1, l d_2) + \text{noise} \quad (43)$$

where $(G_n)_{i,l}$ is the discretized MRF for the n th measurement. Some error is introduced in quantization of the MRFs, but so long as T is small compared to the footprint, this error is

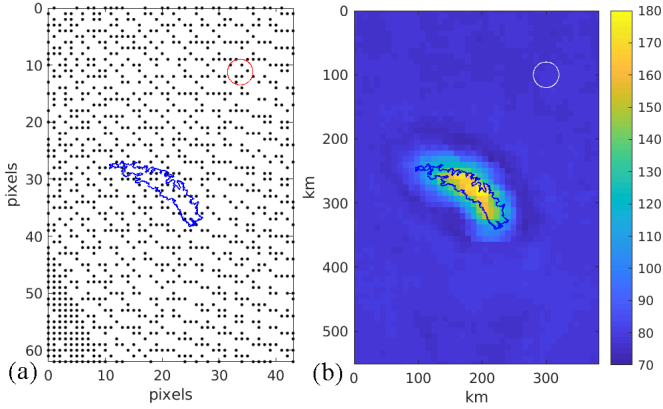


Fig. 10. (a) Measurement center locations. (b) Single day horizontally polarized T_b in K from SMAP data, day 152, 2015 computed using the radiometer form of the Scatterometer Image Reconstruction algorithm [15] on an 8.9-km pixel Lambert Equal Area map projection grid. The ocean is very cool (~ 70 K) while the glacier covered island appears much warmer (~ 180 K); 40-km diameter circles are shown for comparison.

small. Noise is treated as independent of the signal and arises in radiometer measurements from brightness temperature variability and contributions due to the receiver noise figure.

The study target is the island of South Georgia in the South Atlantic at 36.8W 54.4S. Using a Lambert Equal Area map projection centered at the target location, we arbitrarily choose the pixel spacing $T = 8.9$ km because this value is commonly used in Scatterometer Climate Record Pathfinder (SCP) products [16]. The 39 km \times 47 km SMAP 3-dB footprint is thus approximately 4.4×5.3 pixels. Fig. 10(b) illustrates a T_b image of the study area created from a single day (day 150, 2017) of SMAP data while Fig. 10(a) shows the locations of the $N_s = 1079$ measurement MRF centers within the study area. To treat the MRFs as periodic, the SMAP measurement MRFs that overlap an edge of the study area are artificially “wrapped” to extend from the opposite side. Since the ocean is of a nearly uniform temperature, the resulting edge effects from this operation are minimal. For this study area, $N_1 = 44$ and $N_2 = 62$ (approximately 392 km \times 552 km), with $N_N = 2728$. Using $d_1 = d_2 = 2$, $M_1 = 10$, and $M_2 = 15$ ($N_r = 651$) with $E_1 = 1$ and $E_2 = 0$. Fig. 11 shows the corresponding Dirichlet kernel.

Using the sampling locations and the associated measurement-specific MRFs, the \mathbf{C}_v matrix is numerically computed. Two versions are used: the variable aperture case and one where the apertures are assumed to be ideal delta functions. In this simulation, both matrices have full rank (651, the same as N_r) in the band-limited space, but are poorly conditioned with condition numbers of 1.9×10^{17} and 3×10^{16} , respectively. While a good linear algebra solver, e.g., MATLAB, can deal with condition numbers this large, the noise amplification effect can be significant, and so for practical use, regularization is needed when computing the reconstruction. For this study, the regularized pseudo inverse \mathbf{C}_v^\dagger of \mathbf{C}_v is computed as [17]

$$\mathbf{C}_v^\dagger = (\mathbf{C}_v^t \mathbf{C}_v + \alpha \mathbf{I})^{-1} \mathbf{C}_v^t \quad (44)$$

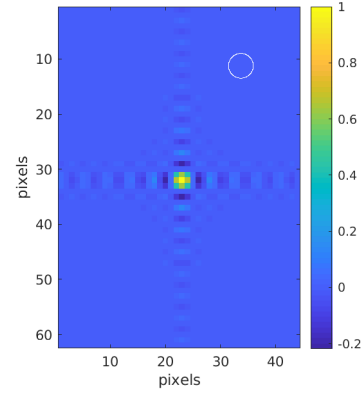


Fig. 11. 2-D Dirichlet function for $N_1 = 44$, $N_2 = 62$, $d_1 = d_2 = 2$, $M_1 = 10$, $M_2 = 15$, $E_1 = 1$, $E_2 = 0$.

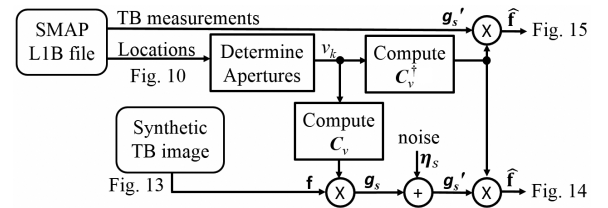


Fig. 12. Diagram of the information flow for the simulation and actual data processing with the figures illustrating information at each point indicated.

where \mathbf{C}_v^t is the transpose of \mathbf{C}_v and α is the regularization parameter discussed later. Using the pseudo inverse also ameliorates inadequate undersampling should it occur (which does not occur in this case). While the signal component of the reconstruction can be exact when $\alpha = 0$, the noise component of the reconstructed image can be very sensitive to noise. Increasing α reduces the noise, but adds distortion to the signal.

To inform the level of regularization required for reconstruction using noisy measurements, simulation is employed. The simulation uses actual MRFs and locations from SMAP L1B files from one day. Fig. 12 illustrates the simulation data flow. The various sampling and reconstruction matrices are numerically computed. The binary-valued synthetic “truth” image is shown in Fig. 13(a). The truth image is ideally lowpass filtered to M_1, M_2 -band-limit it. The true \mathbf{a} is computed using a 2-D fast Fourier transform (FFT). Simulated noise-free measurements are created using 43. Noisy measurements are simulated by adding zero mean, 1.3 K standard deviation Gaussian noise to the simulated noise-free measurements. Results for only a single noise realization are shown. This noise level matches the expected noise level of the SMAP T_b measurements. Because \mathbf{C}_v is full band-limited rank, the reconstruction from the noise-free synthetic measurements for $\alpha = 0$ is exact to within numerical precision, but noisy measurements degrade the reconstruction.

Regularization reduces the effects of noise as illustrated in Fig. 14. Table I summarizes the root mean square (rms) reconstruction error for various choices of the regularization parameter α for the band-limited simulation. (The nonband-limited case in this table is discussed later.) The table reveals

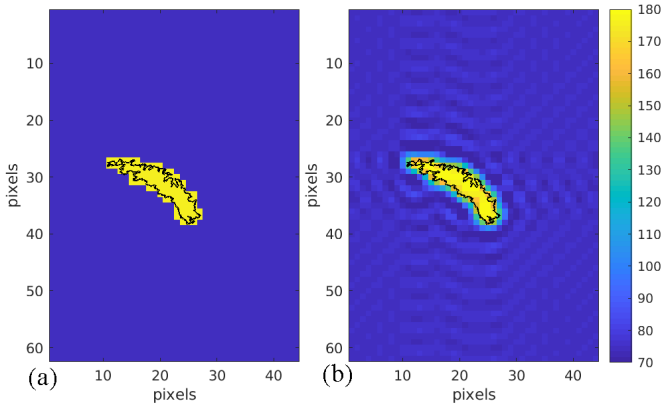


Fig. 13. (a) Binary-valued synthetic truth image created by filling ocean pixels with 70 and land pixels with 180 before and (b) after applying an ideal bandpass filter. The band-limit filter has the negative side effect of introducing Gibb's phenomena "ringing" in the ocean due to the large land/ocean step.

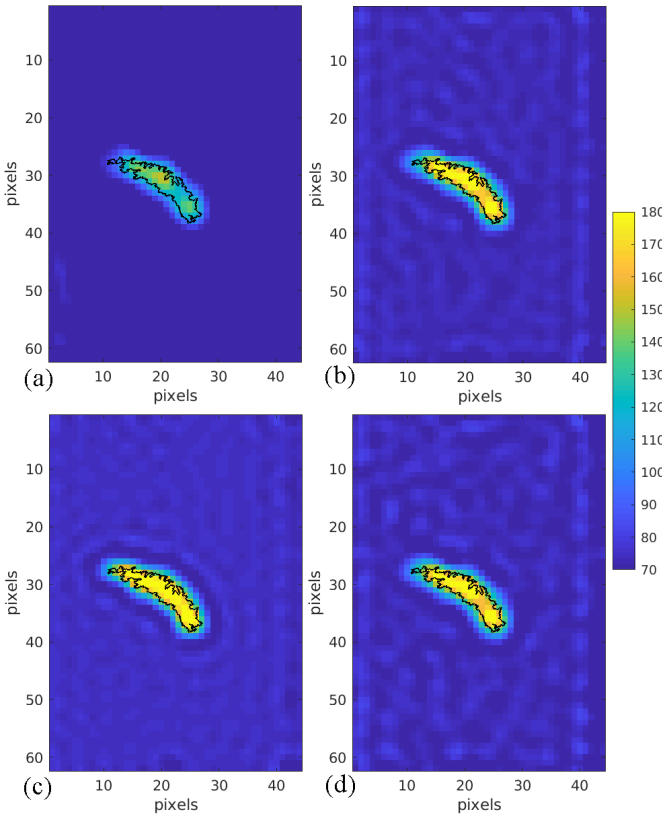


Fig. 14. (a)–(c) Reconstructed T_b images for different values of the regularization parameter α from simulated noisy measurements of the band-limited truth images. (a) $\alpha = 0.001$. (b) $\alpha = 0.01$. (c) $\alpha = 0.1$. (d) Result for noisy measurements for the nonband-limited true image with $\alpha = 0.01$.

that the SMAP noise-level is too high to use nonregularized reconstruction. Based on this table, $\alpha = 0.01$ is chosen for SMAP reconstruction from noisy measurements.

What happens if the true image is not explicitly band-limited? To study this case, the simulation is repeated but using truth image prior to band-limit filtering [Fig. 13(a)]. The resulting reconstructed image, shown in Fig. 15(d), created with $\alpha = 0.01$ from noisy measurements, is nearly identical

TABLE I
RMS DIFFERENCE IN K BETWEEN THE TRUE SYNTHETIC IMAGE, BEFORE AND AFTER BAND-LIMITING, AND THE RECONSTRUCTED IMAGE FROM NOISY AND NOISE-FREE MEASUREMENTS FOR VARIOUS α VALUES

Case	α	Band-Limited	Non-band-limited
Noise-free	0	0	6.1
	0.0001	1.6	5.8
	0.001	2.8	6.2
	0.01	5.1	7.5
	0.1	18.6	19.4
Noisy	0	59.7	60.0
	0.0001	18.1	19.0
	0.001	6.5	8.6
	0.01	5.5	7.8
	0.1	18.6	19.4

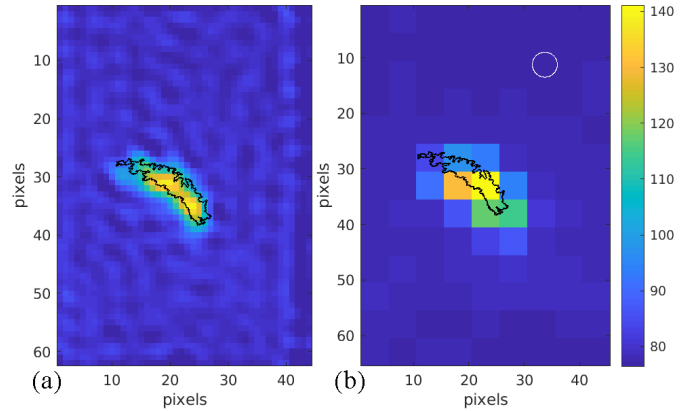


Fig. 15. T_b images from actual data. (a) Reconstructed T_b image for $\alpha = 0.01$ from actual SMAP measurements. (b) Image created by drop-in-the-bucket gridding on a 44.5-km pixel grid. A 40-km diameter circle is shown for comparison. Compare Fig. 10.

to the band-limited true simulation case in Fig. 15(b). This is due in part to the implicit low pass filtering imposed by the aperture function. Table I compares the errors associated with regularization, both band-limited and nonband-limited true images, which have similar errors. We thus find that the restriction imposed by requiring the signal to be band-limited does not significantly impact the actual results.

Turning to actual measurements, Fig. 15(a) shows the reconstructed image using $\alpha = 0.01$ regularization. For comparison a conventionally processed image is shown in Fig. 15(b). This image is created by averaging all the measurements whose center fall within a given 44.5 km pixel, a technique known as drop-in-the-bucket gridding. The averaging in this approach reduces the noise level in the pixel values at the expense of spatial resolution [15], [18]. The reconstructed image clearly better represents the island target compared to the gridded image and exhibits finer resolution compared to the land outline. However, the ocean area in the reconstructed image has more variability than the gridded image. These closely resemble the ocean artifacts observed in the noisy simulation and thus are judged to be an artifact of the reconstruction.

VIII. CONCLUSION

This article has discussed the theory of signal reconstruction from irregularly sampled data with variable apertures where

different measurements may have different aperture functions. This situation is common in microwave sensors where the observations have irregular spacing and different antenna gain patterns resulting in different measurement functions for different measurements.

The reconstruction methods presented in this article enable exact reconstruction of a periodic band-limited signals [1]. For the 1-D case, so long as there is a sufficient number of distinct samples and the aperture function is reasonably well-behaved, a band-limited periodic signal can be exactly reconstructed. In the 2-D case, the situation is more complicated since not all sampling configurations can support full signal reconstruction, even in ideal, noise-free cases. However, so long as the variable aperture function sampling matrix (\mathbf{C}_v or \mathcal{C}_v , depending on dimension) is full rank within the signal bandwidth, the signal can be exactly reconstructed within the limits of numerical precision by inverting a linear system.

Irregular 2-D sampling with an aperture function is explored with a simple toy problem. Then, irregular sampling and reconstruction is illustrated with simulation and actual data using measurements from the SMAP radiometer over a small study area. In simulation, the signal can be exactly recovered from the irregular samples and variable aperture functions, though noise can have an adverse effect. Real data results are consistent with simulation. The results demonstrate that the reconstructed image can provide finer resolution than a conventionally-processed gridded image. The reconstructed signal is sensitive to noise, and in practice some sort of regularization is required. This results in a tradeoff between noise and inaccurate signal reconstruction, and highlights the need for approximate reconstruction methods.

Though most are not designed with variable aperture functions in mind, a variety of reconstruction methods have been developed for the case when only approximate or partially reconstructed results are needed [see [6], [15], [18]–[26] [27]–[29]].

REFERENCES

- [1] D. G. Long and R. O. W. Franz, "Band-limited signal reconstruction from irregular samples with variable apertures," *IEEE Trans. Geosci. Remote Sens.*, vol. 54, no. 4, pp. 2424–2436, Apr. 2016.
- [2] A. V. Oppenheim and A. S. Willsky, *Signals and Systems*. Englewood Cliffs, NJ, USA: Prentice-Hall, 1983.
- [3] M. Unser, "Sampling-50 years after Shannon," *Proc. IEEE*, vol. 88, no. 4, pp. 569–587, Apr. 2000.
- [4] K. Gröchenig, "Reconstruction algorithms in irregular sampling," *Math. Comput.*, vol. 59, no. 199, pp. 181–194, 1992.
- [5] K. Gröchenig, "A discrete theory of irregular sampling," *Linear Algebra Appl.*, vol. 193, pp. 129–150, Nov. 1993.
- [6] D. S. Early and D. G. Long, "Image reconstruction and enhanced resolution imaging from irregular samples," *IEEE Trans. Geosci. Remote Sens.*, vol. 39, no. 2, pp. 291–302, Feb. 2001.
- [7] P. J. Davis, *Interpolation Approximation*. Mineola, NY, USA: Dover, 2014.
- [8] L. Pfister and Y. Bresler, "Bounding multivariate trigonometric polynomials," *IEEE Trans. Signal Process.*, vol. 67, no. 3, pp. 700–707, Feb. 2019.
- [9] P. J. Olver. (Apr. 6, 2016). *On Multivariate Interpolation*. [Online]. Available: <https://www-users.math.umn.edu/olver/n/mv.pdf>
- [10] A. Zygmund, *Trigonometric Series*. Cambridge, U.K.: Cambridge Univ. Press, 2005.
- [11] T. Sørveik and M. A. Nome, "Trigonometric interpolation on lattice grids," *BIT Numer. Math.*, vol. 56, pp. 256–341, 2015. [Online]. Available: <https://link.springer.com/article/10.1007/s10543-015-0562-0>
- [12] H. R. Kunsch, E. Agrell, and F. A. Hamprecht, "Optimal lattices for sampling," *IEEE Trans. Inf. Theory*, vol. 51, no. 2, pp. 634–647, Feb. 2005.
- [13] F. T. Ulaby and D. G. Long, *Microwave Radar and Radiometric Remote Sensing*. Ann Arbor, MI, USA: Univ. of Michigan Press, 2014.
- [14] J. Piepmeier, P. Mohammed, G. De Amici, E. Kim, J. Pen and C. Ruff. Algorithm Theoretical Basis Document: SMAP Calibrated, Time-ordered Brightness Temperatures L1B_TB Data Product. SMAP Project, Rev. A. Dec. 10, 2014. [Online]. Available: https://smap.jpl.nasa.gov/system/internal_resources/details/original/278_L1B_TB_RevA_web.pdf
- [15] D. G. Long, M. J. Brodzik, and M. A. Hardman, "Enhanced-resolution SMAP brightness temperature image products," *IEEE Trans. Geosci. Remote Sens.*, vol. 57, no. 7, pp. 4151–4163, Jul. 2019.
- [16] (2020). *Scatterometer Climate Record Pathfinder*. [Online]. Available: <https://www.scp.byu.edu/>
- [17] A. A. Tikhonov and V. Y. Arsenin, *Solution Ill-Posed Problems*. Washington, DC, USA: Winston & Sons, 1977.
- [18] D. G. Long and M. J. Brodzik, "Optimum image formation for spaceborne microwave radiometer products," *IEEE Trans. Geosci. Remote Sens.*, vol. 54, no. 5, pp. 2763–2779, May 2016, doi: 10.1109/TGRS.2015.2505677.
- [19] D. G. Long, "Comparison of SeaWinds backscatter imaging algorithms," *IEEE J. Sel. Topics Appl. Earth Observ. Remote Sens.*, vol. 10, no. 5, pp. 2214–2231, May 2017.
- [20] M. Foster, "An application of the wiener-kolmogorov smoothing theory to matrix inversion," *J. Soc. Ind. Appl. Math.*, vol. 9, no. 3, pp. 387–392, Sep. 1961.
- [21] Y. Censor, "Finite series-expansion reconstruction methods," *Proc. IEEE*, vol. 71, no. 3, pp. 409–419, Mar. 1983.
- [22] H. G. Feichtinger and K. Gröchenig, "Iterative reconstruction of multivariate band-limited functions from irregular sampling values," *SIAM J. Math. Anal.*, vol. 23, no. 1, pp. 244–261, Jan. 1992.
- [23] H. G. Feichtinger, K. Gröchenig, and T. Strohmer, "Efficient numerical methods in non-uniform sampling theory," *Numerische Mathematik*, vol. 29, pp. 433–440, 1995. [Online]. Available: <https://link.springer.com/article/10.1007%2Fs002110050101>
- [24] P. L. Butzer and J. Lei, "Approximation of signals using measured sampled values and error analysis," *Commun. Appl. Anal.*, vol. 4, no. 2, pp. 245–255, 2000.
- [25] W. Sun and X. Zhou, "Reconstruction of band-limited signals from local averages," *IEEE Trans. Inf. Theory*, vol. 48, no. 11, pp. 2955–2963, Nov. 2002.
- [26] M. Migliaccio and F. Bruno, "A new interpolation kernel for SAR interferometric registration," *IEEE Trans. Geosci. Remote Sens.*, vol. 41, no. 5, pp. 1105–1110, May 2003.
- [27] M. Migliaccio, F. Nunziata, F. Bruno, and F. Casu, "Knab sampling window for InSAR data interpolation," *IEEE Trans. Geosci. Remote Sens. Lett.*, vol. 4, no. 3, pp. 397–400, Jul. 2011.
- [28] X. Xu, W. Ye, and A. Entezari, "Bandlimited reconstruction of multidimensional images from irregular samples," *IEEE Trans. Image Process.*, vol. 22, no. 10, pp. 3950–3960, Oct. 2013.
- [29] F. Lenti, F. Nunziata, C. Estatico, and M. Migliaccio, "On the spatial resolution enhancement of microwave radiometer data in banach spaces," *IEEE Trans. Geosci. Remote Sens.*, vol. 52, no. 3, pp. 1834–1842, Mar. 2014.